Z_2 Dirac points with topologically protected multihelicoid surface states

Tiantian Zhang [1,2,*] Daisuke Hara,[1] and Shuichi Murakami [1,2,†]

[1]*Department of Physics, Tokyo Institute of Technology, Ookayama, Meguro-ku, Tokyo 152-8551, Japan*

[2]*Tokodai Institute for Element Strategy, Tokyo Institute of Technology, Nagatsuta, Midori-ku, Yokohama, Kanagawa 226-8503, Japan*

(Received 8 April 2022; accepted 15 August 2022; published 31 August 2022)

In some Dirac systems with time-reversal ($\mathcal{T}$) and glide ($\mathcal{G}$) symmetries, multihelicoid surface states (MHSSs) appear, as discussed in various systems such as electronic and photonic ones. However, the topological nature and the conditions for the appearance of the MHSSs have not been understood. Here we show that MHSSs result from bulk-surface correspondence for the Z_2 monopole charge $\mathcal{Q}$, which *cannot* be defined as a local quantity associated with the Dirac point, unlike the Z monopole charge characterizing Weyl points. The previously known formula of $\mathcal{Q}$ turns out to be non-gauge-invariant and thus cannot characterize the MHSSs. This shortcoming of the definition of $\mathcal{Q}$ is amended by redefining $\mathcal{Q}$ as a global topological invariant in k-space. Surprisingly, the newly defined $\mathcal{Q}$, characterizing $\mathcal{GT}$ invariant gapless systems, is equal to the $\mathcal{G}$-protected Z_2 topological invariant ν, which is nontrivial only in $\mathcal{T}$-breaking gapped systems. This global definition of $\mathcal{Q}$ automatically guarantees the appearance of MHSSs even when the Dirac point splits into Weyl points or a nodal ring by lowering the symmetry, as long as the $\mathcal{GT}$ symmetry is preserved. $\mathcal{Q}$ can be simplified to symmetry-based indicators when two vertical $\mathcal{G}$s are preserved, and filling-enforced topological crystalline insulators are diagnosed in several cases when a $\mathcal{T}$-breaking perturbation is induced. Material candidate $Li_2B_4O_7$ together with a list of space groups preserving MHSSs are also proposed.

DOI: 10.1103/PhysRevResearch.4.033170

I. INTRODUCTION

Since the first proposal of the $\mathcal{T}$-protected topological insulator in 2005 [1–3], a vast number of topological (crystalline) insulators (TI/TCI) have been discovered in gapped band structures with different symmetries [4–11]. The topological equivalence of two systems can be diagnosed by either the type or the value of the topological invariants, associated with diverse topological surface states due to bulk-surface correspondence (BSC). For example, TIs associated with surface Dirac cone(s) are proposed with topological invariant $z_2 = 1$ in Ref. [3]. As for topological semimetals, their band degeneracies are protected by various topological invariants associated with disparate BSC, such as the Berry phase γ for the nodal line/ring with drumhead surface states [12–16], the Z-type monopole charge $\mathcal{C}$ for Weyl points with helical surface states [17–26], and Z_2-type monopole charge $\mathcal{Q}$ for Dirac points with MHSSs such as double (quad-)helicoid surface states (DHSSs/QHSSs) [21,27–32]. In particular, DHSSs/QHSSs associated with Dirac points realized in $\mathcal{GT}$-preserving systems are particularly interesting. Because they originate from Dirac points, which are composites of a pairs of Weyl points with $\mathcal{C} = \pm 1$, they can escape from gap opening only under some conditions. Nevertheless, these conditions have not been identified because their topological nature has not been understood yet. Therefore, it is not known how to realize DHSSs/QHSSs in general systems, such as electronic and photonic systems. Furthermore, two more topological invariants ν [29,33] and μ_2 [34] can be defined in terms of $\mathcal{G}$ when the system is fully gapped, but there has been no research studying their relationships with $\mathcal{Q}$ so far.

In this paper, we point out that the previous definition of the Z_2 monopole charge $\mathcal{Q}$ is not gauge-invariant, and we show a new gauge-invariant definition for $\mathcal{Q}$. Thereby, we can show the BSC between nontrivial values of $\mathcal{Q}$ and MHSSs. In Sec. II, we start the discussion for conventional Dirac points composed of two Weyl points with opposite $\mathcal{C}$ in Dirac semimetal systems, in which no gapless helical surface states are guaranteed, and then we discuss Z_2 Dirac points carrying monopole charge $\mathcal{Q}$ protected by $\tilde{\Theta}$ in Secs. III A and IV B. Here, we give an amended gauge-invariant definition of $\mathcal{Q}$. We also show that the Z_2 monopole charge $\mathcal{Q}$ associated with Dirac points under $\mathcal{G}$ and $\mathcal{T}$ symmetry cannot be defined as a local quantity, as opposed to previous works, and surprisingly it is equal to ν, which characterizes a $\mathcal{G}$-protected TCI phase without $\mathcal{T}$-symmetry in Sec. III B. With this newly defined gauge-invariant $\mathcal{Q}$ ($=\nu$), we establish BSC for Dirac points with both DHSSs and QHSSs for $\mathcal{GT}$-preserving systems in Secs. III D and IV C. This global definition of $\mathcal{Q}$ automatically guarantees the appearance of MHSSs even when the Dirac point splits into Weyl points or a nodal ring by lowering the symmetry, as long as the $\mathcal{GT}$ symmetry is preserved. We find that QHSSs can only be retained in spinless systems,

*zhang.t.ac@m.titech.ac.jp
†murakami@stat.phys.titech.ac.jp

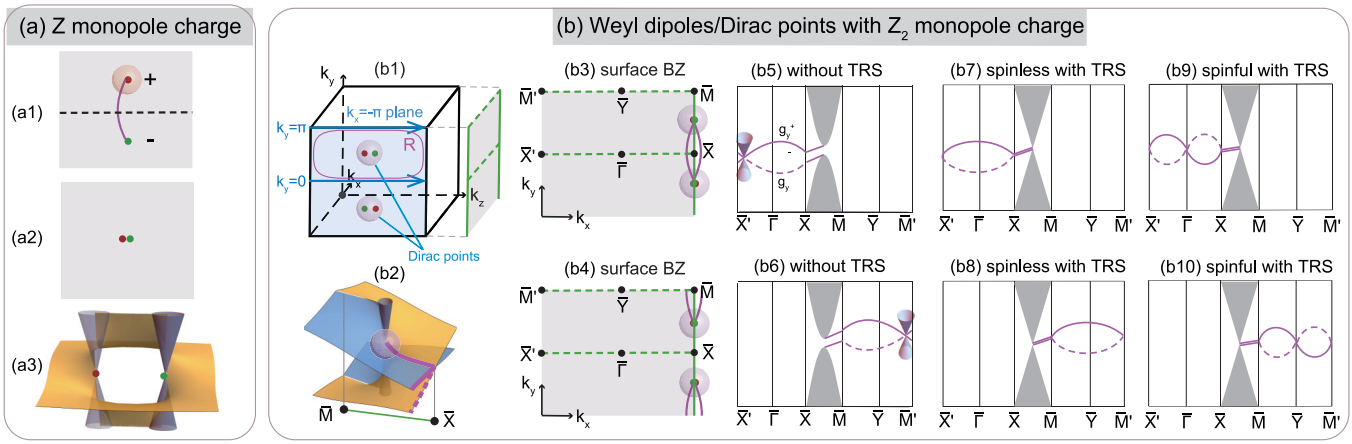

FIG. 1. Z_2 Dirac points under $\mathcal{G}$- and $\mathcal{T}$-symmetries and associated DHSSs. (a1) Fermi arcs for Weyl points with opposite monopole charges $\mathcal{C}$, which can be defined either by the sphere enclosed by the Weyl point or by a two-dimensional plane marked by the dashed line. (a2) Fermi arcs do not necessarily exist for a conventional Dirac point composed of a pair of Weyl points with opposite $\mathcal{C}$. (a3) Helical surface states for a pair of Weyl points carrying opposite $\mathcal{C}$. (b1) Locations for Z_2 Dirac points (Weyl dipoles) on the $k_x = -\pi$ plane (blue plane) satisfying $\tilde{\Theta}_y^2 = -1$ in the bulk BZ. (b2) Double-helicoid surface states contributed by Z_2 Dirac points, which will be projected along $\bar{M}$-$\bar{X}$ on the surface BZ. The gray cone is the bulk Z_2 Dirac band. Blue and yellow sheets are the anticrossing helical surface states. Purple lines show the surface-state connections along $\bar{\Gamma}$-$\bar{X}$-$\bar{M}$ directions. (b3) Fermi arcs for Z_2 Dirac points (Weyl dipoles) on the $\mathcal{G}_y$-preserved surface BZ, which corresponds to the gray plane shown in (b1). The Fermi arcs will change to (b4) when the energy changes. (b5),(b6) Two possible surface-state connections with $\nu_y = 1$ ($=\nu_y^{\text{surface}}$) in the $\mathcal{T}$-breaking system defined by single $\mathcal{G}_y$, with the single surface Dirac cone located along different $\mathcal{G}_y$-invariant lines. TRS denotes time-reversal symmetry. (b7),(b8) Two possible topological surface-state connections for Z_2 Dirac points in the spinless and $\mathcal{T}$-preserving case. (b9),(b10) Two possible topological surface-state connections for Z_2 Dirac points in the spinful and $\mathcal{T}$-preserving case. Surface states shown in (b7)–(b10) are all in the double-helicoid shape shown in (b2).

and it vanishes in spinful systems due to the ill-defined $\mathcal{Q}$ in Sec. IV. The first Z_2 Dirac material candidate $Li_2B_4O_7$ and a list of space groups with QHSSs will be offered in Sec. V. Therefore, our theory has established conditions to guarantee DHSSs/QHSSs, which can lead to their realization in a broad range of physical systems.

II. MONOPOLE CHARGES $\mathcal{C}$ FOR WEYL AND DIRAC POINTS

Monopole charge $\mathcal{C}$ can be defined by the Chern number on a sphere enclosing the Weyl point, or on a two-dimensional (2D) plane in the 3D Brillouin zone (BZ) marked by the dashed line in Fig. 1(a1). The former definition shows the local property of $\mathcal{C}$, while the latter offers the global topology to understand the influence of $\mathcal{C}$ on the whole BZ, giving rise to gapless surface states connecting two Weyl points with opposite $\mathcal{C}$, as shown in Fig. 1(a3). Fermi arcs are isoenergetic surface states, and they can disappear when those two Weyl points are projected onto the same momentum on the surface BZ or when they are forced to coalesce into a Dirac point by additional symmetries [35–56], as shown by the purple solid line in Figs. 1(a1) and 1(a2).

Although the monopole charge $\mathcal{C}$ will vanish for a Dirac point [27,35,57–59], a new Z_2 topological invariant $\mathcal{Q}$ can be defined when an antiunitary operator $\tilde{\Theta} = \mathcal{G}\mathcal{T}$ with $\tilde{\Theta}^2 = -1$ is present [21], and its corresponding topological bulk degeneracies are named Z_2 Weyl dipoles or Z_2 Dirac points (detailed discussions on Weyl dipoles are in [60]). Z_2 Dirac points always appear in pairs and are located at $\mathcal{T}$-related momenta in the BZ. Since Z_2 Weyl dipoles and Z_2 Dirac points can be transformed mutually by $\tilde{\Theta}$-preserved perturbations, we will use Z_2 Dirac points as an example to show the global topology of $\mathcal{Q}$ in the following.

III. MONOPOLE CHARGE $\mathcal{Q}$ IN SYSTEMS WITH A SINGLE $\mathcal{G}\mathcal{T}$

In this section, we will show that the definition of Z_2 monopole charge $\mathcal{Q}$ given in Ref. [21] in systems with a single $\mathcal{G}$ and $\mathcal{T}$ actually depends on a gauge, and we will redefine $\mathcal{Q}$ in a gauge-independent way. This eventually shows that $\mathcal{Q}$ cannot be defined locally in k-space, but that $\mathcal{Q}$ shows global topology in k-space.

A. Redefinition of monopole charge $\mathcal{Q}$

We consider systems with one glide symmetry $\mathcal{G}_y = \{M_y|\frac{1}{2}00\}$, where M_y represents the mirror reflection with respect to the xz plane. Systems with only a $\mathcal{G}_y$ symmetry correspond to no. 7, and their BZs are shown in both Figs. 1(b1) and 2(a). Let $\tilde{\Theta}_y$ denote an antiunitary operator $\tilde{\Theta}_y = \mathcal{T}\mathcal{G}_y$, which leads to $\tilde{\Theta}_y^2 = e^{-ik_x}$. Therefore, $k_x = +\pi/-\pi$ is a special plane where $\tilde{\Theta}_y^2 = -1$ is satisfied, as shown by the blue plane in Fig. 1(b1) and the green plane (region $\mathcal{A}$) in Figs. 2(a)–2(c), and here we consider the case with two Z_2 Dirac points on the $k_x = -\pi$ plane in the 3D BZ. They are related by $\mathcal{T}$ symmetry, and so they cannot appear at time-reversal-invariant momenta (TRIM). Thus, Z_2 Dirac points are usually located on high-symmetry lines for systems with only one $\mathcal{G}$.

Here, we consider a Dirac point on the $\tilde{\Theta}$-invariant line with $\tilde{\Theta}^2 = -1$, i.e., the E-A or D-B line on the $k_x = -\pi$ plane shown in Fig. 2(c). A Z_2 monopole charge $\mathcal{Q}$ is associated

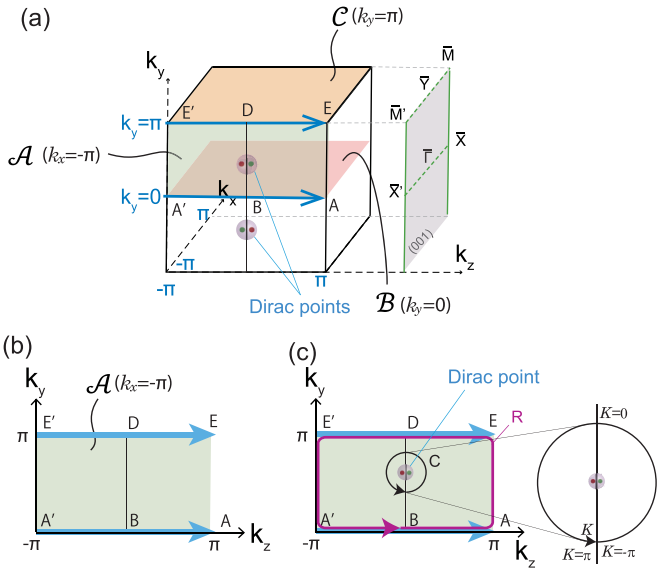

FIG. 2. (a) Brillouin zone for the space group no. 7, which only has a glide symmetry, and the colored planes are used for the calculation of ν. Projection onto the (001) plane is also shown. The regions $\mathcal{A}$, $\mathcal{B}$, and $\mathcal{C}$ are defined by $\mathcal{A} = \{\mathbf{k}|k_x = -\pi, 0 \leqslant k_y \leqslant \pi, -\pi \leqslant k_z \leqslant \pi\}$, $\mathcal{B} = \{\mathbf{k}|k_x = 0, -\pi \leqslant k_y \leqslant \pi, -\pi \leqslant k_z \leqslant \pi\}$, and $\mathcal{C} = \{\mathbf{k}|k_x = \pi, -\pi \leqslant k_y \leqslant \pi, -\pi \leqslant k_z \leqslant \pi\}$. (b) Slice of the Brillouin zone at $k_x = -\pi$. If the system has both time-reversal and glide symmetries, the Z_2 invariant ν is shown to be equal to the difference of $\tilde{\Theta}$-polarization, calculated as a Berry phase along the two blue lines. (c) When the system has a Dirac point either on the DB line or on the EA line, and is gapped in the rest of the region $\mathcal{A}$, the Z_2 monopole charge $\mathcal{Q}$ for the Dirac point can be well defined. In the previous work, $\mathcal{Q}$ is defined along the circle C parametrized. To guarantee the gauge invariance of $\mathcal{Q}$, we need to deform the circle C to the rectangle R (purple line), which makes $\mathcal{Q}$ equal to ν.

with the Dirac point, defined in terms of wave functions on a $\tilde{\Theta}$-symmetric sphere enclosing the Dirac point, according to Ref. [21]. The formulation of $\mathcal{Q}$ closely follows that of the Z_2 topological invariant for time-reversal invariant topological insulators without inversion symmetry [61], but with a replacement of $\mathcal{T}$ by $\tilde{\Theta}$:

$$(-1)^{\mathcal{Q}} = \frac{\mathrm{Pf}[W(0)]}{\sqrt{\det[W(0)]}} \frac{\mathrm{Pf}[W(\pi)]}{\sqrt{\det[W(\pi)]}}, \tag{1}$$

where the matrix $W_{mn}(K)$ is defined by

$$W_{mn}(K) = \langle u_m(-K)|\tilde{\Theta}|u_n(K)\rangle, \tag{2}$$

with m and n running over the occupied bands [21]. Here we have introduced a coordinate K ($-\pi \leqslant K \leqslant \pi$) along the circle C, as shown in Fig. 2(c), so that $\tilde{\Theta}$ transforms K to $-K$. It was claimed that $\mathcal{Q} \pmod 2$ is gauge-invariant in Ref. [21]; nevertheless, we point out that this discussion of gauge invariance is not correct. As opposed to the discussion in the Methods section of Ref. [21], some gauge transformation (e.g., multiplying a phase factor e^{iK} to one eigenstate) changes the branch choice of the square root in Eq. (1) and will alter the value of $\mathcal{Q}$ by unity. Thus, we hereby reexamine the definition of the Z_2 monopole charge $\mathcal{Q}$.

Similar to the $\mathcal{T}$-polarization [61], we note here that the crucial condition for $\mathcal{Q}$ is $\tilde{\Theta}^2 = -1$, which is satisfied on the plane $k_x = -\pi$. Thus, among the wave functions on the sphere surrounding the Dirac point, only those on the circle C lying on the $k_x = -\pi$ plane are relevant for the definition in Eq. (1). Since there is a gauge transformation for wave functions along circle C, which will change $\mathcal{Q}$ by unity (see the last paragraph of Sec. III B in Ref. [61]), this definition is not sufficient to cause the Z_2 monopole charge $\mathcal{Q}$ to be well-defined.

To make the value of $\mathcal{Q}$ gauge-independent modulo 2, we need to make some constraints on the gauge choice. It is achieved by imposing that the gauge of the wave functions is continuous within the region $\mathcal{A}$. It allows us to enlarge the circle C to a rectangle R in a $\tilde{\Theta}$-symmetric way in the definition of $\mathcal{Q}$ [see Figs. 1(b1) and 2(c)]. This is possible only when the bulk band structure on $k_x = -\pi$ is gapped except for the Dirac points considered. Since wave functions should be periodic along the k_z direction, i.e., equal between the two edges of the rectangle, EA and E′A′, the above gauge transformation altering $\mathcal{Q}$ by unity is now prohibited. Under this gauge condition, similarly to the argument for inversion-asymmetric Z_2 TIs in Ref. [61], the Z_2 monopole charge is rewritten to be a difference in "$\tilde{\Theta}$-polarization" between $k_y = 0$ and $k_y = \pi$, and we conclude

$$\mathcal{Q} = P_{\tilde{\Theta}}(k_y = \pi) - P_{\tilde{\Theta}}(k_y = 0) \pmod 2, \tag{3}$$

where $P_{\tilde{\Theta}}(k_y) = \frac{1}{2\pi}(\gamma_{\mathrm{L}}^{+} - \gamma_{\mathrm{L}}^{-})$. γ_{L} is the Berry phase with the integral path L taken as $k_y = 0$ and $k_y = \pi$ lines on the $k_x = -\pi$ plane, and "$\pm$" represent the sectors with positive or negative glide eigenvalues for the Bloch wave functions. We call $P_{\tilde{\Theta}}(k_y)$ $\tilde{\Theta}$-polarization because $\tilde{\Theta}_y$ switches those two glide sectors, in analogy to the time-reversal polarization in Ref. [61]. Thus, as opposed to previous works, $\mathcal{Q}$ can *only* be defined globally in k-space in Eq. (12). This is in strong contrast with the locally defined monopole charge $\mathcal{C}$ for Weyl points.

To summarize, we found that the definition of the Z_2 monopole charge $\mathcal{Q}$ for the Dirac point in a previous work in terms of wave functions on a circle C surrounding the Dirac point is gauge-dependent and ill-defined. To make $\mathcal{Q}$ well-defined, we need to impose a condition that the system is gapped everywhere in the region $\mathcal{A}$ ($k_x = -\pi, -\pi \leqslant k_z \leqslant \pi$, $0 \leqslant k_y \leqslant \pi$), except for the Dirac point. Under this condition, the Z_2 monopole charge is now well-defined in terms of wave functions along the rectangle R. In this sense, the Z_2 monopole charge cannot be defined locally but has a global nature. We also note that a simplified formula for $\mathcal{Q}$ in systems with an additional twofold rotation or screw symmetry is given in terms of eigenvalues of those rotation symmetries in Ref. [21], but it is valid only when the system satisfies the conditions discussed above.

All the discussions above are in spinless systems, and we note that the definition of $\mathcal{Q}$ remains the same in spinful systems because $\tilde{\Theta}^2 = e^{-ik_x}$ remains true also in spinful systems with single glide symmetry. We further notice that $\mathcal{Q}$ is equal to the global $\mathcal{G}$-protected Z_2 topological invariant ν mathematically and physically in both spinless and spinful systems, which will be discussed in detail in the next section.

B. Topological invariant ν for gapped systems with $\mathcal{G}$

In spinless systems with glide symmetry $\mathcal{G}_y = \{M_y|\frac{1}{2}00)\}$, eigenstates on glide-invariant planes $k_y = 0$ and $k_y = \pi$ are classified into two glide sectors with

$$g_\pm(k_x) = \pm e^{-ik_x/2}. \tag{4}$$

For three-dimensional (3D) spinless systems with a gapped band structure, a Z_2-type topological invariant [29,33,62] can be defined by the glide symmetry as

$$\begin{aligned}\nu = \frac{1}{2\pi}\Bigg[&\int_{\mathcal{A}} F_{yz}dk_ydk_z + \int_{\mathcal{B}} F^-_{zx}dk_zdk_x \\ &- \int_{\mathcal{C}} F^-_{zx}dk_zdk_x\Bigg] \\ &- \frac{1}{\pi}(\gamma^+_{\mathrm{A'BA}} + \gamma^+_{\mathrm{EDE'}}) \pmod 2,\end{aligned} \tag{5}$$

where $\mathcal{A}$, $\mathcal{B}$, and $\mathcal{C}$ are the integral regions shown in Fig. 2(a). In this formula, we have defined the Berry connections

$$\boldsymbol{A}(\boldsymbol{k}) \equiv \sum_{n\in\mathrm{occ}} i\,\langle u_{n\boldsymbol{k}}|\,\nabla_{\boldsymbol{k}}\,|u_{n\boldsymbol{k}}\rangle\,, \tag{6}$$

$$\boldsymbol{A}^\pm(\boldsymbol{k}) \equiv \sum_{n\in\mathrm{occ}} i\,\langle u^\pm_{n\boldsymbol{k}}|\,\nabla_{\boldsymbol{k}}\,|u^\pm_{n\boldsymbol{k}}\rangle\,, \tag{7}$$

and the corresponding Berry curvatures

$$F_{ij}(\boldsymbol{k}) = \partial_{k_i}A_j(\boldsymbol{k}) - \partial_{k_j}A_i(\boldsymbol{k}), \tag{8}$$

$$F^\pm_{ij}(\boldsymbol{k}) = \partial_{k_i}A^\pm_j(\boldsymbol{k}) - \partial_{k_j}A^\pm_i(\boldsymbol{k}), \tag{9}$$

where the summation $\sum_{n\in\mathrm{occ}}$ is over the occupied states with band index n, and $|u^\pm_{n\boldsymbol{k}}\rangle$ are the Bloch wave functions within the positive/negative glide sectors of $g_\pm(k_x) = \pm e^{-ik_x/2}$. The Berry phase $\gamma^\pm(\boldsymbol{k})$ is defined along a closed path λ as

$$\gamma^\pm_\lambda(\boldsymbol{k}) = \oint_\lambda \boldsymbol{A}^\pm(\boldsymbol{k})\cdot d\boldsymbol{k}. \tag{10}$$

In Eq. (5), $\gamma^+_{\mathrm{A'BA}}$ and $\gamma^+_{\mathrm{EDE'}}$ are Berry phases with the paths λ taken as straight lines with $\mathrm{A'} \to \mathrm{B} \to \mathrm{A}$ and $\mathrm{E} \to \mathrm{D} \to \mathrm{E'}$, respectively, where the corresponding high-symmetry points are shown in Fig. 2. We note that the wave functions are periodic along the k_z direction. It is noted that for convenience, we take the glide operation to be $\mathcal{G}_y = \{M_y|\frac{1}{2}00\}$, which is different from $\{M_y|00\frac{1}{2}\}$ taken in Refs. [29,33,62].

We now consider systems with time-reversal symmetry ($\mathcal{T}$). In this case, integrals on the $\mathcal{B}$ and $\mathcal{C}$ surface will vanish, because the Berry curvature will change its sign, while the glide sector will be unchanged under $\mathcal{T}$. The integral on $\mathcal{A}$ is rewritten as

$$\int_{\mathcal{A}} F_{yz}dk_ydk_z = \gamma_{\mathrm{A'BA}} + \gamma_{\mathrm{EDE'}}, \tag{11}$$

where the gauge of the wave functions is taken to be continuous between $k_z = -\pi$ and $k_z = \pi$. Thus, Eq. (5) can be written as

$$\begin{aligned}\nu &= \frac{1}{2\pi}(\gamma^-_{\mathrm{A'BA}} - \gamma^+_{\mathrm{A'BA}} + \gamma^-_{\mathrm{EDE'}} - \gamma^+_{\mathrm{EDE'}}) \\ &= P_{\tilde\Theta}(k_y = \pi) - P_{\tilde\Theta}(k_y = 0) \pmod 2,\end{aligned} \tag{12}$$

where we define

$$P_{\tilde\Theta}(k_y) = \frac{1}{2\pi}(\gamma^+_{\mathrm{L}} - \gamma^-_{\mathrm{L}}) \ (k_y = 0, \pi), \tag{13}$$

with $\mathrm{L} = (\mathrm{A'BA}, \mathrm{E'DE})$ being a straight path along the k_x direction with fixed $k_y(= 0, \pi)$ on the $k_x = -\pi$ plane. It is a polarization difference between two glide sectors along the 1D subspaces marked by the blue arrows in Fig. 2(b). The antiunitary symmetry $\tilde\Theta \equiv G_y\mathcal{T}$ gives rise to double degeneracy on the DB and EA lines due to $\tilde\Theta^2 = -1$. Then the glide sectors on the $k_x = -\pi$ plane are switched by $\tilde\Theta$.

Next, we show that the definition of Eq. (13) can be extended to arbitrary values of k_y ($0 < k_y < \pi$). By classifying eigenstates of occupied states into two sets I and II, where the two sets are mutually transformed by $\tilde\Theta$, we define

$$P_{\tilde\Theta}(k_y) = \frac{1}{2\pi}\left(\gamma^{\mathrm{I}}_{\mathrm{L}} - \gamma^{\mathrm{II}}_{\mathrm{L}}\right) \ (0 \leqslant k_y \leqslant \pi). \tag{14}$$

This is reduced to Eq. (13) for $k_y = 0, \pi$. We note that $\tilde\Theta$-polarization is an integer, and so is ν. Since $\mathcal{T}$-polarization is gauge-dependent [61], $\tilde\Theta$-polarization will also be. However, the difference of $\tilde\Theta$-polarization between $k_y = 0$ and $k_y = \pi$ is defined in terms of modulo 2, which is gauge-independent due to the continuous gauge choice on the $\mathcal{A}$ plane.

Therefore, when the system is fully gapped and $\mathcal{T}$-symmetric, $P_{\tilde\Theta}(k_y)$ is a quantized integer and a continuous function of k_y. Thus, from Eq. (12), ν vanishes in gapped systems with $\mathcal{T}$ as discussed in Refs. [29,33]. In other words, the $\mathcal{G}$-protected TCI phase requires breaking of $\mathcal{T}$-symmetry.

C. Topological invariant ν for Dirac systems with $\mathcal{G}$ and $\mathcal{T}$

Although this $\mathcal{G}$-protected topological invariant ν is originally defined for fully gapped systems, we propose that it can be extended to gapless systems with $\mathcal{T}$ by Eq. (12), as long as the system is gapped along the two paths A′BA and EDE′ in Eq. (12). For example, by adding a twofold rotation along the y axis, doubly degenerate states can cross along the E-A line or the D-B line, and the system become gapless, which is the case considered in Ref. [21]. In this case, ν can be nontrivial even when $\mathcal{T}$ is preserved, and $\mathcal{Q}$ is equal to the global $\mathcal{G}$-protected Z_2 topological invariant ν mathematically and physically in both the spinless and spinful systems:

$$\mathcal{Q} = \nu. \tag{15}$$

This is counterintuitive since ν is originally defined for fully gapped systems and it vanishes when the system is $\mathcal{T}$-invariant [29,33], while $\mathcal{Q}$ is associated with the Dirac point in $\mathcal{T}$-preserving gapless systems. We propose in this paper that ν is also well-defined by Eq. (12), even for gapless systems, as long as the system is fully gapped along the two blue lines marked in Fig. 1(b1). It is nontrivial when the system is $\mathcal{T}$-invariant and has Dirac cones on the $\bar{M}$-$\bar{X}$ line. The nontrivial $\mathcal{Q}$ ($=\nu$) results in topological surface states on the $\mathcal{G}_y$-preserving (001) surface, which will be discussed in the next subsection.

D. BSC for $\mathcal{Q}$ with a single $\mathcal{G}$

Observing topological states on the surface is the simplest and most straightforward way to demonstrate the topology of

the bulk states, due to the BSC. Here we establish BSC for a nonzero $\mathcal{Q}$ with a single $\mathcal{G}$ in both the spinless and spinful systems. In the present case, two Dirac points are projected onto the $\bar{M}$-$\bar{X}$ line satisfying $\tilde{\Theta}_y^2 = -1$. The Fermi energy is set at the Dirac point. In this subsection, we will show that Fermi arcs for a nonzero $\mathcal{Q}$ have two possibilities shown in Figs. 1(b3) and 1(b4) on the $\mathcal{G}_y$-preserved surface BZ, where the surface states extend either toward $\bar{M}$ or $\bar{X}$. The green dashed lines are glide-invariant ones, and the green solid lines are $\tilde{\Theta}_y$-invariant ones, with $\tilde{\Theta}_y^2 = -1$, giving rise to double degeneracy for surface states.

In gapped systems with $\mathcal{G}_y$ symmetry, the bulk Z_2 topological invariant ν_y is well-defined, and by the BSC it is equal to the surface Z_2 topological invariant ν_y^{surface} which characterizes how the surface states cross the Fermi energy (see Sec. S1 of the Supplemental Material for details [60]). However, in the present gapless system, ν_y remains well-defined by Eq. (12), while ν_y^{surface} becomes ill-defined due to the bulk gap closing along $\bar{M}$-$\bar{X}$. To establish BSC in the present gapless system, first we break the $\mathcal{T}$ symmetry slightly to open a small bulk gap at the Dirac point. Figures 1(b5) and 1(b6) are two possible nontrivial surface-state connections with $\nu_y^{\text{surface}} = 1$ in gapped band structures without $\mathcal{T}$ [29,33], which has a single unpinned surface Dirac cone along the glide-invariant lines, $\bar{M}$-$\bar{Y}$-$\bar{M}'$ or $\bar{X}$-$\bar{\Gamma}$-$\bar{X}'$, but not both. Next, we cause the $\mathcal{T}$-breaking perturbation to be zero; all the states along $\bar{X}$-$\bar{M}$ then becomes doubly degenerate due to $\tilde{\Theta}^2 = -1$, resulting in two kinds of possible surface-state connections, both without SOC [Figs. 1(b7) and 1(b8)] and with SOC [Figs. 1(b9) and 1(b10)]. The corresponding Fermi arcs are shown in Figs. 1(b3) and 1(b4). Remarkably, the doubly degenerate surface states should start exactly at the Dirac point, belonging to the DHSSs shown in Fig. 1(b2). These DHSSs can be interpreted as a superposition of surface states from two Weyl points with opposite $\mathcal{C}$, and their intersections are protected along $\bar{X}$-$\bar{M}$ by $\tilde{\Theta}_y^2 = -1$ in both the spinless and spinful systems. Such DHSSs also have a Z_2 nature, which directly follows from the Z_2 nature of ν in gapped systems [29,33]. For example, when there are two Dirac points within $0 < k_y < \pi$ on the $k_x = -\pi$ plane, two sets of DHSSs are expected, but they can be annihilated by a continuous change of surface states without changing the bulk bands.

IV. $\mathcal{Q}$ WITH TWO VERTICAL $\mathcal{G}$s IN SPINLESS SYSTEMS

Z_2 Dirac systems with two $\tilde{\Theta}$ have more unresolved mysteries, and we find that $\mathcal{Q}$ is well-defined *only* in the spinless systems, which is beyond people's expectation [21]. In this section, we will show that when additional crystalline symmetries such as an additional vertical glide symmetry are present, $\mathcal{Q}$ $(=\nu)$ can be in the form of a symmetry-based indicator calculated in terms of irreducible representations at high-symmetry points.

For example, systems with no. 110 have two glide symmetries perpendicular to each other, i.e., $\mathcal{G}_x = \{M_x|0\frac{1}{2}0\}$ and $\mathcal{G}_y = \{M_y|00\frac{1}{2}\}$. Those two vertical glide symmetries lead to $\tilde{\Theta}_x^2 = -1$ at $k_y = \pi$ and $\tilde{\Theta}_y^2 = -1$ at $k_z = \pi$, resulting in Z_2 Dirac points at non-TRIM high-symmetry points, e.g., P and P'. The original formula for the Z_2 glide invariant ν is expressed as a sum of integrals in k-space, but it can be simplified as C_{2z} eigenvalues due to the existence of $\mathcal{G}_x$ and $\mathcal{G}_y$ [63,64], which will be explained in detail in the following subsection.

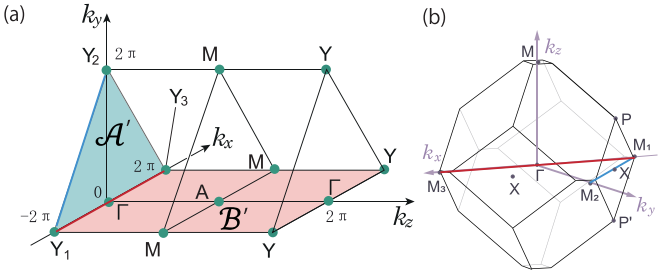

FIG. 3. Brillouin zones for no. 9 and no. 110 used in the calculation of the glide-Z_2 invariant ν_y. (a) Half of the Brillouin zone of the space group no. 9. (b) Brillouin zone of the space group no. 110. Blue and red lines are the paths for the Berry phases used in the calculation of ν_y.

A. Z_2 topological invariant ν for the $\mathcal{G}$-protected TCI phase for space group no. 110

Under the glide symmetry $\mathcal{G}_y = \{M_y|00\frac{1}{2}\}$, the Z_2 glide invariant ν characterizing the TCI phase protected by glide symmetry is written as a sum of integral terms within k space. It has been shown that ν can be in an expression of a symmetry-based indicator by adding an additional inversion symmetry, i.e., by considering space groups no. 13, no. 14, and no. 15, which is calculated only by the irreducible representations at high-symmetry points [62–64].

Here, we focus on spinless systems with space group no. 110, which has two glide symmetries $\mathcal{G}_x = \{M_x|00\frac{1}{2}\}$ and $\mathcal{G}_y = \{M_y|00\frac{1}{2}\}$. In no. 110, we can define two $\mathcal{G}$-protected topological invariants ν_x and ν_y associated with $\mathcal{G}_x$ and $\mathcal{G}_y$, respectively. In the following, we will show that ν_x and ν_y are equal and given by $n/2$ mod 2, where n is the number of occupied bands. Since no. 110 is a body-centered-tetragonal lattice, the formula of ν here will be greatly different from that in primitive lattices. Thus, we will start with the formula of ν_y for the $\mathcal{G}_y$ on no. 9 having the base-centered lattice as follows [64]:

$$\nu_y = \frac{1}{2\pi}\left[\int_{\mathcal{A}'} F_{xy}dk_xdk_y + \int_{\mathcal{B}'}\left(\frac{1}{2}F_{zx} - F_{zx}^{+}\right)dk_zdk_x\right] + \frac{1}{\pi}\left(\gamma_{Y_1Y_2} - \gamma_{Y_1Y_3}^{+}\right), \tag{16}$$

where $\mathcal{A}' = \{\boldsymbol{k}|k_z = 0,\ 0 < k_y, k_x + k_y < 2\pi, k_y - k_x < 2\pi\}$ and $\mathcal{B}' = \{\boldsymbol{k}|k_y = 0, -2\pi < k_y < 2\pi, 0 < k_z < 2\pi\}$ are depicted in Fig. 3(a) and $Y_1(-2\pi, 0, 0)$, $Y_2(0, 2\pi, 0)$, and $Y_3(2\pi, 0, 0)$. Here the formula is altered with a shift along the k_z direction by π from that in Ref. [64] for convenience.

To obtain the formula for no. 110, we first make a coordinate transformation from the base-centered lattice to the body-centered-tetragonal lattice. This is straightforward because no. 9 is a subgroup of no. 110 Then with the other glide symmetry $\mathcal{G}_x$, we show that three surface-integral terms vanish

by symmetry constraints, with the remaining term as

$$\nu_y = \frac{1}{\pi}\left(\gamma_{M_1M_2} - \gamma^+_{M_1M_3}\right), \tag{17}$$

where $M_1(-2\pi, 0, 0)$, $M_2(0, 2\pi, 0)$, and $M_3(2\pi, 0, 0)$ are TRIM of no. 110 [see Fig. 3(b)]. In spinless systems, we can utilize the C_{2z} symmetry as a result of $\mathcal{G}_x$ and $\mathcal{G}_y$ symmetries. (Such a rule is broken in the spinful case, which is because the commutation relations between $\mathcal{G}_x$ and $\mathcal{G}_y$ change. This is consistent with the ill-definedness of $\mathcal{Q}$ in spinful systems with two glide symmetries.) Since C_{2z} and $\mathcal{G}_y$ commute with each other, we can evaluate $e^{i\pi\nu_y}$ via the sewing matrix below:

$$(-1)^{\nu_y} = \prod_i \frac{\zeta_i(M)}{\zeta_i(X)} \frac{\zeta_i^+(\Gamma)}{\zeta_i^+(M)}. \tag{18}$$

Here ζ is the C_{2z} eigenvalues and ζ^+ is the C_{2z} eigenvalues for the $\mathcal{G}_x = +e^{-ik_z/2}$ sector. Because M and Γ are on the common C_{2z} invariant line, they share the same C_{2z} and $\mathcal{G}_x$ eigenvalue. Thus, ν_y can be simplified as

$$(-1)^{\nu_y} = \prod_i \frac{\zeta_i(\Gamma)}{\zeta_i(X)}. \tag{19}$$

We note that there are two inequivalent X points for no. 110, but we do not need to distinguish them in Eq. (19) because they are on the same C_{2z} axis due to the nonprimitive nature of the lattice. Therefore, we obtain

$$\nu_x = \nu_y, \tag{20}$$

and we can simply write $\nu = \nu_x = \nu_y$ in the following. In fact, this formula is equal to the symmetry-based indicator μ_2 for $\mathcal{T}$-breaking spinless systems with no. 27 ($Pcc2$) having two glide symmetries $\mathcal{G}_x$ and $\mathcal{G}_y$, given by Ref. [34]

$$\mu_2 = \frac{1}{4} \sum_{\mathbf{k}:\ \text{TRIMs at } k_z=0} (n^+_{\mathbf{k}} - n^-_{\mathbf{k}}). \tag{21}$$

We can directly show $\mu_2 = \nu$ as follows. In no. 27, there are four TRIM on $k_z = 0$: $\tilde{\Gamma}$ (0,0,0), $\tilde{M}$ $(\pi, \pi, 0)$, $\tilde{X}$ $(\pi, 0, 0)$, $\tilde{Y}$ $(0, \pi, 0)$. The Brillouin zone for no. 27 is half of that for no. 110, and each of these four TRIM in no. 27 corresponds to two k points in no. 110, i.e., $\tilde{X}$ point (and also $\tilde{Y}$) corresponds to two non-TRIM points in no. 110. Such correspondence shows that two states with $C_{2z} = 1$ and -1 present in no. 27 will give no contribution to μ_2. The $\tilde{M}$ point corresponds to X $(\pi, \pi, 0)$ and X' $(-\pi, \pi, 0)$ in no. 110, which are in fact on the common C_{2z} axis, sharing the same C_{2z} eigenvalue. Similarly, $\tilde{\Gamma}$ point corresponds to Γ (0,0,0) and M $(2\pi, 0, 0)$ in no. 110, which are also on the common C_{2z} axis, sharing the same C_{2z} eigenvalue. Thus, we obtain

$$\begin{aligned}\mu_2 &= \tfrac{1}{4}\{2(n^+_\Gamma - n^-_\Gamma) + 2(n^+_X - n^-_X)\} \\ &\equiv -(n^-_\Gamma + n^-_X) \ (\text{mod } 2),\end{aligned} \tag{22}$$

from which $\mu_2 = \nu$ follows.

At Γ, there are four 1D irreps $\Gamma_1, \ldots, \Gamma_4$ with $C_{2z} = 1$ and one 2D irrep Γ_5 with two states having $C_{2z} = -1$. Thus, all the irreps contribute trivially to the product of ν. On the other hand, the irrep at the X point is a 2D one with opposite C_{2z} eigenvalues, therefore the product for ν is equal to

$$\nu = N/2 \quad (\text{mod } 2), \tag{23}$$

where N is the number of occupied bands. Thus, ν is nontrivial when $N = 4m + 2$ (m is an integer) and trivial when $N = 4m$.

In fact, it is also discussed in Ref. [34] that ν is solely determined by the filling of the system in no. 106 and no. 110, which are supergroups of no. 27. The topological nature of this topologically nontrivial phase has not been understood so far [34]. However, as shown in our paper, this symmetry-based indicator μ_2 is in fact the $\mathcal{G}$-protected topological invariants ν_x and ν_y. In this subsection, we have shown these properties for gapped systems. In the next subsection, we will see them also for gapless systems.

TABLE I. Spinless systems with Z_2 Dirac points associated with QHSSs.

Space group	Two vertical glide mirrors	Location	Momenta used for Eq. (19)
no. 73	$\{M_x\|\frac{1}{2}, \frac{1}{2}, 0\}$; $\{M_y\|\frac{1}{2}, 0, 0\}$	W	Γ, T
no. 110	$\{M_x\|\frac{1}{2}, \frac{1}{2}, 0\}$; $\{M_y\|\frac{1}{2}, \frac{1}{2}, 0\}$	P	Γ, X
no. 142	$\{M_x\|\frac{1}{2}, \frac{1}{2}, 0\}$; $\{M_y\|\frac{1}{2}, 0, 0\}$	P	Γ, X
no. 206	$\{M_x\|\frac{1}{2}, \frac{1}{2}, 0\}$; $\{M_y\|\frac{1}{2}, 0, 0\}$	P	Γ, N
no. 228	$\{M_x\|\frac{1}{2}, \frac{3}{4}, 0\}$; $\{M_y\|\frac{3}{4}, \frac{1}{2}, 0\}$	W	Γ, X
no. 230	$\{M_x\|\frac{1}{2}, \frac{1}{2}, 0\}$; $\{M_y\|\frac{1}{2}, 0, 0\}$	P	Γ, N

B. Topological invariant ν (=$\mathcal{Q}$) for the Dirac semimetal phase with two vertical $\mathcal{G}$s

When time-reversal symmetry is preserved in space group no. 110, the states are always fourfold degenerate at the momenta of Z_2 Dirac point. Thus, one cannot have a gap with $n = 4m + 2$ (m is an integer). A $\mathcal{T}$-breaking perturbation is required for the topological crystalline insulator (TCI) phase with nontrivial ν, as we discussed in the previous section. Thus we consider the case in which the $\mathcal{T}$ is slightly broken to open a tiny bulk gap, where we can safely apply the bulk-surface correspondence for the $\mathcal{G}$-protected topological invariants ν_x and ν_y.

In the present case of gapless systems, ν in Eq. (12) is ill-defined because of the presence of the bulk Dirac point on the blue lines in Fig. 1(b1), but instead we can use Eq. (19) to safely define ν. Equation (19) is a new formula for $\mathcal{Q}(=\nu)$ calculated by the symmetry data at TRIM, and as we have seen, it is also equal to the symmetry-based indicator μ_2 in Eq. (22). μ_2 is also entangled with filling-enforced topological crystalline insulators when there is a full gap of the system, because μ_2 is related to the filling N by $\mu_2 \equiv N/2$ (mod 2) in space group no. 110. Therefore, insulators with $N = 4m + 2$ (mod 2) (m is an integer) are nontrivial in no. 110 [64].

We note that Eq. (19) still holds for other space groups listed in Table I with proper high-symmetry momenta. Furthermore, only no. 73, no. 110, and no. 142 can be converted to filling-enforced topological crystalline insulators when $\mathcal{T}$-symmetry is broken.

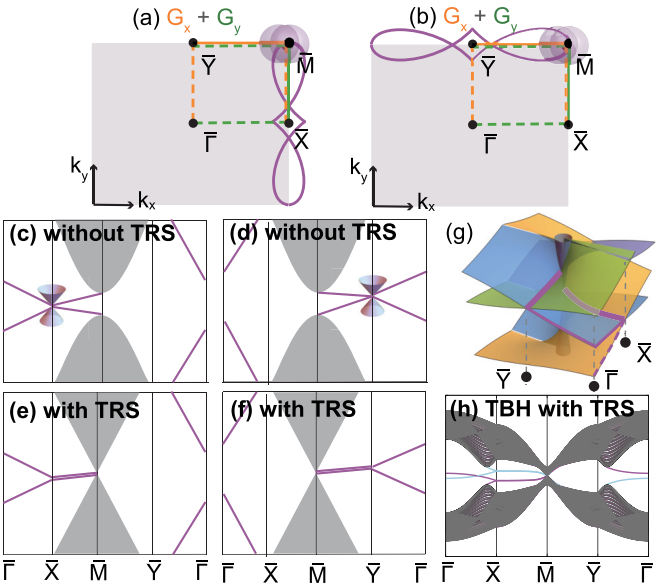

FIG. 4. Z_2 Dirac points with $\mathcal{T}$- and two vertical $\mathcal{G}$-symmetries and associated QHSSs. (a) Locations and Fermi arcs for Z_2 Dirac points on the surface BZ preserving $\mathcal{G}_x$ and $\mathcal{G}_y$. Green (orange) dashed/solid lines are $\mathcal{G}_{y(x)}$-invariant/$\tilde{\Theta}^2_{y(x)} = -1$ lines. Purple solid lines are Fermi arcs, which will change to (b) when the energy changes. (c), (d) Two possible surface-state connections for quad-helicoid surface states after breaking $\mathcal{T}$, which corresponds to topological crystalline insulators with two nontrivial $\mathcal{G}$-protected topological invariants $\nu_x{=}\nu_y{=}1$. Surface Dirac cones located at $\bar{X}$ in (c) and $\bar{Y}$ in (d) will evolve to QHSSs contributed by nontrivial $\mathcal{Q}$ in (e) and (f), respectively. (e), (f) Two different surface-state connections in $\mathcal{T}$-preserving systems with nontrivial $\mathcal{Q}$, which correspond to the Fermi arcs shown in (a) and (b), respectively. TRS denotes time-reversal symmetry. (g) Illustration for quad-helicoid surface states, where the purple lines show the gapless nature of the surface states along $\bar{Y}$-$\bar{\Gamma}$-$\bar{X}$ directions. (h) Surface-states calculation obtained by the tight-binding model for no. 110 with two vertical glide symmetries, where two Z_2 Dirac points are projected onto $\bar{M}$. Purple and blue lines represent the surface states from the top surface and bottom surface of the slab, which show quantum spin-Hall-like flows along $\bar{Y}$-$\bar{\Gamma}$-$\bar{X}$ directions, resulting in quad-helicoid surface states.

C. BSC for $\mathcal{Q}$ with two vertical $\mathcal{G}$s in spinless systems

Now we will show BSC for $\mathcal{Q}$ with two vertical $\mathcal{G}$, similarly to cases with one $\mathcal{G}$ in Sec. III D. Figures 4(a) and 4(b) show the surface BZ on the (001) surface preserving two vertical $\mathcal{G}$. In $\mathcal{T}$-preserving spinless systems with two vertical $\mathcal{G}$, Z_2 Dirac points are projected to $\bar{M}$ on the (001) surface BZ, which makes ν_x^{surface} and ν_y^{surface} ill-defined. By borrowing similar analysis on systems with one $\mathcal{G}$, first we introduce a $\mathcal{T}$-breaking perturbation to open a small gap for Z_2 Dirac points to make ν_x^{surface} and ν_y^{surface} well-defined and be equal to $\nu_x(=\nu_y)$, which will give rise to two possible nontrivial surface-state connections with a single surface Dirac cone pinned at $\bar{X}$ and $\bar{Y}$, respectively, as summarized in Figs. 4(c) and 4(d). Next, when the $\mathcal{T}$ symmetry is restored, doubly degenerate surface states along the surface BZ boundaries protected by $\tilde{\Theta}_x^2 = -1 = \tilde{\Theta}_y^2$ will appear. The corresponding surface-state connections for QHSSs along high-symmetry lines are shown in Figs. 4(e) and 4(f).

Here, doubly degenerate surface states also start exactly from the Dirac point at $\bar{M}$ and connect either to $\bar{X}$ or to $\bar{Y}$ with the protection of $\tilde{\Theta}_y^2 = -1$ or $\tilde{\Theta}_x^2 = -1$ along the BZ boundaries. Away from the $\bar{M}$-$\bar{X}$ or $\bar{M}$-$\bar{Y}$ line, this degeneracy will be split toward the conduction and valence bands, showing the QHSSs with two quantum spin Hall (QSH) -like flows along $\bar{Y}$-$\bar{\Gamma}$-$\bar{X}$ directions, as marked by the purple lines in Fig. 4(g). This conclusion is supported by our tight-binding model calculation for no. 110 shown in Fig. 4(h), where the purple (blue) lines represent the surface states obtained from the top (bottom) of the slab (see Sec. S1 of the Supplemental Material for details [60]). The surface-state filling at $\bar{X}/\bar{M}$ and $\bar{X}'/\bar{M}'$ will be changed by 1 when the surface states cross through the Z_2 Dirac points, showing the helicoid nature of the surface states.

In spinful systems with two vertical $\mathcal{G}$s, $\mathcal{Q}$ for the bulk Dirac point is ill-defined because of the presence of other bulk degeneracies at TRIM on the $\tilde{\Theta}^2 = -1$ planes, in contrast to spinless systems. Therefore, the BSC will also be eliminated.

Thus we have shown that the Z_2 monopole charge $\mathcal{Q}$ characterizing MHSSs only has a global nature in k-space, and it is not a local quantity. This automatically guarantees that the MHSSs will survive perturbations that split the Dirac point into a nodal ring or a pair of Weyl points, as seen in the following material example.

V. Z_2 DIRAC MATERIAL $Li_2B_4O_7$ WITH QHSSs

QHSSs are the consequence of BSC for Z_2 Dirac points with two vertical $\mathcal{G}$, as well as the bridge for connecting $\mathcal{Q}$, ν, and μ_2. By following Table I, we propose an experimentally synthesized material candidate $Li_2B_4O_7$ with no. 110 [65] and two Z_2 Dirac fermions in its spinless electronic band structure, associated with QHSSs. As shown in Figs. 5(a) and 5(c), all the fourfold band crossings at P and P' are Z_2 Dirac points, which will be projected onto the corner point $\bar{M}$ on the (001) surface. Figure 5(b) is the surface-state calculation on the (001) surface, following the k-path marked in Fig. 5(d). Two groups of anticrossing helical surface states with different Fermi velocity (chirality) together with degenerate surface states along surface BZ boundaries show the QHSSs feature of $Li_2B_4O_7$.

QHSSs can also be obtained in systems with Z_2 Weyl dipoles. After breaking C'_{4z} symmetry, the symmetry of $Li_2B_4O_7$ is lowered to no. 45 and two Z_2 Dirac points split into two pairs of Z_2 Weyl dipoles along the k_z direction, i.e., $W_1 + W_2$ and $W'_1 + W'_2$, respectively, as shown in Figs. 5(b) and 5(d). Since $\tilde{\Theta}_x$ and $\tilde{\Theta}_y$ are still preserved in no. 45, each pair of Weyl dipole will also carry a nonzero $\mathcal{Q}$ and lead to QHSSs on the (001) surface, as shown in Figs. 5(g) and 5(h), which are quite similar to those from two Z_2 Dirac points. Within a pair of Weyl dipoles, W_1 and W_2 cannot be annihilated with each other due to the nonzero $\mathcal{Q}$, although their total monopole charge $\mathcal{C}$ is zero, which is different from general Weyl semimetals.

VI. CONCLUSION

We present a full understanding of the topology of $\mathcal{GT}$-protected Z_2 Dirac points in this paper. We offer the

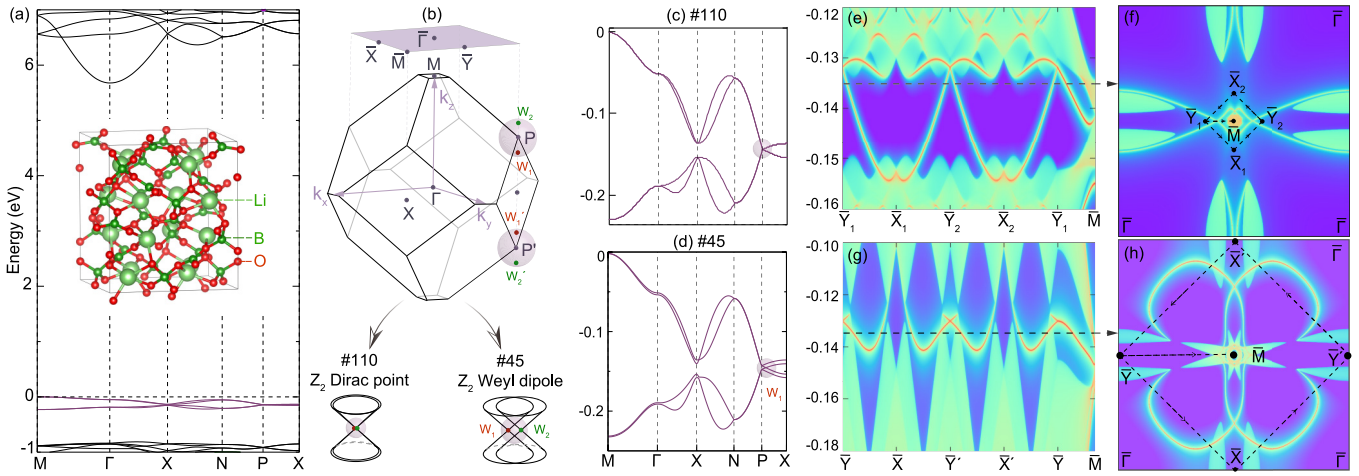

FIG. 5. (a) Crystal structure and band structure for $Li_2B_4O_7$. (b) BZ and surface BZ for both no. 110 and no. 45 along the [001] direction. (c), (d) Spinless band structure of $Li_2B_4O_7$ for no. 110 and no. 45, respectively. Parts (e), (f) and (g), (h) are QHSSs calculated on the (001) surface for no. 110 and no. 45, respectively, where the k paths in (e) and (g) are marked by the black dashed lines in (f) and (h), respectively. Parts (f) and (h) are the Fermi arcs calculated around two Z_2 Dirac points located at $\bar{M}$.

gauge-invariant formula for Z_2 monopole charge $\mathcal{Q}$ protected by $(\mathcal{GT})^2 = -1$, and we find that $\mathcal{Q}$ can only be defined globally in k-space. $\mathcal{Q}$ can be formulated into a simpler form in terms of irreducible representations at two high-symmetry momenta when two vertical $\mathcal{G}$s are present. DHSSs can be obtained in both spinless and spinful systems with one $\mathcal{G}$, while QHSSs can only be obtained in spinless systems with two vertical $\mathcal{G}$. QHSSs in spinless Z_2 Dirac systems are also the bridge to unify $\mathcal{GT}$-protected $\mathcal{Q}$, $\mathcal{G}$-protected ν, $\mathcal{G}$-protected symmetry-based indicator μ_2, and even filling-enforced topological crystalline insulators. We also offer a material candidate $Li_2B_4O_7$ and a list of space groups having QHSSs.

ACKNOWLEDGMENTS

We acknowledge the support from Tokodai Institute for Element Strategy (TIES) funded by MEXT Elements Strategy Initiative to Form Core Research Center Grants No. JPMXP0112101001, No. JP18J23289, No. JP18H03678, and No. JP22H00108. T.Z. also acknowledges the support by Japan Society for the Promotion of Science (JSPS), KAKENHI Grant No. JP21K13865.

[1] C. L. Kane and E. J. Mele, Z_2 Topological Order and the Quantum Spin Hall Effect, Phys. Rev. Lett. **95**, 146802 (2005).
[2] B. A. Bernevig, T. L. Hughes, and S.-C. Zhang, Quantum spin Hall effect and topological phase transition in HgTe quantum wells, Science **314**, 1757 (2006).
[3] L. Fu, C. L. Kane, and E. J. Mele, Topological Insulators in Three Dimensions, Phys. Rev. Lett. **98**, 106803 (2007).
[4] A. P. Schnyder, S. Ryu, A. Furusaki, and A. W. W. Ludwig, Classification of topological insulators and superconductors in three spatial dimensions, Phys. Rev. B **78**, 195125 (2008).
[5] A. Kitaev, *Periodic Table for Topological Insulators and Superconductors*, AIP Conf. Proc. No. 1134 (American Institute of Physics, New York, 2009), pp. 22–30.
[6] C.-K. Chiu, J. C. Y. Teo, A. P. Schnyder, and S. Ryu, Classification of topological quantum matter with symmetries, Rev. Mod. Phys. **88**, 035005 (2016).
[7] H. C. Po, A. Vishwanath, and H. Watanabe, Symmetry-based indicators of band topology in the 230 space groups, Nat. Commun. **8**, 50 (2017).
[8] B. Bradlyn, L. Elcoro, J. Cano, M. G. Vergniory, Z. Wang, C. Felser, M. I. Aroyo, and B. A. Bernevig, Topological quantum chemistry, Nature (London) **547**, 298 (2017).
[9] Z. Song, T. Zhang, Z. Fang, and C. Fang, Quantitative mappings between symmetry and topology in solids, Nat. Commun. **9**, 3530 (2018).
[10] Z. Song, T. Zhang, and C. Fang, Diagnosis for Nonmagnetic Topological Semimetals in the Absence of Spin-Orbital Coupling, Phys. Rev. X **8**, 031069 (2018).
[11] E. Khalaf, H. C. Po, A. Vishwanath, and H. Watanabe, Symmetry Indicators and Anomalous Surface States of Topological Crystalline Insulators, Phys. Rev. X **8**, 031070 (2018).
[12] A. A. Burkov, M. D. Hook, and L. Balents, Topological nodal semimetals, Phys. Rev. B **84**, 235126 (2011).
[13] C. Fang, H. Weng, X. Dai, and Z. Fang, Topological nodal line semimetals, Chin. Phys. B **25**, 117106 (2016).
[14] G. Bian, T. R. Chang, H. Zheng, S. Velury, S. Y. Xu, T. Neupert, C. K. Chiu, S. M. Huang, D. S. Sanchez, I. Belopolski, N. Alidoust, P. J. Chen, G. Chang, A. Bansil, H. T. Jeng, H. Lin, and M. Z. Hasan, Drumhead surface states and topological nodal-line fermions in $TlTaSe_2$, Phys. Rev. B **93**, 121113(R) (2016).
[15] Y.-H. Chan, C.-K. Chiu, M. Y. Chou, and A. P. Schnyder, Ca_3P_2 and other topological semimetals with line nodes and drumhead surface states, Phys. Rev. B **93**, 205132 (2016).

[16] W. Deng, J. Lu, F. Li, X. Huang, M. Yan, J. Ma, and Z. Liu, Nodal rings and drumhead surface states in phononic crystals, Nat. Commun. **10**, 1769 (2019).

[17] H. Weng, C. Fang, Z. Fang, B. A. Bernevig, and X. Dai, Weyl Semimetal Phase in Noncentrosymmetric Transition-Metal Monophosphides, Phys. Rev. X **5**, 011029 (2015).

[18] B. Q. Lv, H. M. Weng, B. B. Fu, X. P. Wang, H. Miao, J. Ma, P. Richard, X. C. Huang, L. X. Zhao, G. F. Chen, Z. Fang, X. Dai, T. Qian, and H. Ding, Experimental Discovery of Weyl Semimetal TaAs, Phys. Rev. X **5**, 031013 (2015).

[19] S.-Y. Xu, I. Belopolski, N. Alidoust, M. Neupane, G. Bian, C. Zhang, R. Sankar, G. Chang, Z. Yuan, C.-C. Lee *et al.*, Discovery of a Weyl fermion semimetal and topological fermi arcs, Science **349**, 613 (2015).

[20] X. Wan, A. M. Turner, A. Vishwanath, and S. Y. Savrasov, Topological semimetal and Fermi-arc surface states in the electronic structure of pyrochlore iridates, Phys. Rev. B **83**, 205101 (2011).

[21] C. Fang, L. Lu, J. Liu, and L. Fu, Topological semimetals with helicoid surface states, Nat. Phys. **12**, 936 (2016).

[22] B. Yang, Q. Guo, B. Tremain, R. Liu, L. E. Barr, Q. Yan, W. Gao, H. Liu, Y. Xiang, J. Chen *et al.*, Ideal Weyl points and helicoid surface states in artificial photonic crystal structures, Science **359**, 1013 (2018).

[23] W.-J. Chen, M. Xiao, and C. T. Chan, Photonic crystals possessing multiple Weyl points and the experimental observation of robust surface states, Nat. Commun. **7**, 13038 (2016).

[24] H. He, C. Qiu, X. Cai, M. Xiao, M. Ke, F. Zhang, and Z. Liu, Observation of quadratic Weyl points and double-helicoid arcs, Nat. Commun. **11**, 1820 (2020).

[25] T. Zhang, Z. Song, A. Alexandradinata, H. Weng, C. Fang, L. Lu, and Z. Fang, Double-Weyl Phonons in Transition-Metal Monosilicides, Phys. Rev. Lett. **120**, 016401 (2018).

[26] T. Zhang, R. Takahashi, C. Fang, and S. Murakami, Twofold quadruple Weyl nodes in chiral cubic crystals, Phys. Rev. B **102**, 125148 (2020).

[27] B.-J. Yang and N. Nagaosa, Classification of stable three-dimensional Dirac semimetals with nontrivial topology, Nat. Commun. **5**, 4898 (2014).

[28] T. Morimoto and A. Furusaki, Weyl and Dirac semimetals with Z_2 topological charge, Phys. Rev. B **89**, 235127 (2014).

[29] K. Shiozaki, M. Sato, and K. Gomi, Z_2 topology in nonsymmorphic crystalline insulators: Mobius twist in surface states, Phys. Rev. B **91**, 155120 (2015).

[30] E. V. Gorbar, V. A. Miransky, I. A. Shovkovy, and P. O. Sukhachov, Surface Fermi arcs in Z_2 Weyl semimetals A_3Bi (A = Na, K, Rb), Phys. Rev. B **91**, 235138 (2015).

[31] X. Cai, L. Ye, C. Qiu, M. Xiao, R. Yu, M. Ke, and Z. Liu, Symmetry-enforced three-dimensional Dirac phononic crystals, Light: Sci. Appl. **9**, 1 (2020).

[32] H. Cheng, Y. Sha, R. Liu, C. Fang, and L. Lu, Discovering Topological Surface States of Dirac Points, Phys. Rev. Lett. **124**, 104301 (2020).

[33] C. Fang and L. Fu, New classes of three-dimensional topological crystalline insulators: Nonsymmorphic and magnetic, Phys. Rev. B **91**, 161105(R) (2015).

[34] S. Ono and H. Watanabe, Unified understanding of symmetry indicators for all internal symmetry classes, Phys. Rev. B **98**, 115150 (2018).

[35] Z. Wang, Y. Sun, X.-Q. Chen, C. Franchini, G. Xu, H. Weng, X. Dai, and Z. Fang, Dirac semimetal and topological phase transitions in A_3Bi (A = Na, K, Rb), Phys. Rev. B **85**, 195320 (2012).

[36] Z. K. Liu, B. Zhou, Y. Zhang, Z. J. Wang, H. M. Weng, D. Prabhakaran, S.-K. Mo, Z. X. Shen, Z. Fang, X. Dai *et al.*, Discovery of a three-dimensional topological Dirac semimetal, Na_3Bi, Science **343**, 864 (2014).

[37] M. Neupane, S.-Y. Xu, R. Sankar, N. Alidoust, G. Bian, C. Liu, I. Belopolski, T.-R. Chang, H.-T. Jeng, H. Lin *et al.*, Observation of a three-dimensional topological Dirac semimetal phase in high-mobility Cd_3As_2, Nat. Commun. **5**, 3786 (2014).

[38] Z. K. Liu, J. Jiang, B. Zhou, Z. J. Wang, Y. Zhang, H. M. Weng, D. Prabhakaran, S. K. Mo, H. Peng, P. Dudin *et al.*, A stable three-dimensional topological Dirac semimetal Cd_3As_2, Nat. Mater. **13**, 677 (2014).

[39] S. Borisenko, Q. Gibson, D. Evtushinsky, V. Zabolotnyy, B. Büchner, and R. J. Cava, Experimental Realization of a Three-Dimensional Dirac Semimetal, Phys. Rev. Lett. **113**, 027603 (2014).

[40] J. A. Steinberg, S. M. Young, S. Zaheer, C. L. Kane, E. J. Mele, and A. M. Rappe, Bulk Dirac Points in Distorted Spinels, Phys. Rev. Lett. **112**, 036403 (2014).

[41] S. Zhang, Q. Wu, L. Schoop, M. N. Ali, Y. Shi, N. Ni, Q. Gibson, S. Jiang, V. Sidorov, W. Yi *et al.*, Breakdown of three-dimensional dirac semimetal state in pressurized Cd_3As_2, Phys. Rev. B **91**, 165133 (2015).

[42] S.-Y. Xu, C. Liu, S. K. Kushwaha, R. Sankar, J. W. Krizan, I. Belopolski, M. Neupane, G. Bian, N. Alidoust, T.-R. Chang *et al.*, Observation of fermi arc surface states in a topological metal, Science **347**, 294 (2015).

[43] H. Wang, L. Xu, H. Y. Chen, and J.-H. Jiang, Three-dimensional photonic Dirac points stabilized by point group symmetry, Phys. Rev. B **93**, 235155 (2016).

[44] P. Tang, Q. Zhou, G. Xu, and S.-C. Zhang, Dirac fermions in an antiferromagnetic semimetal, Nat. Phys. **12**, 1100 (2016).

[45] M. Kargarian, M. Randeria, and Y.-M. Lu, Are the surface Fermi arcs in Dirac semimetals topologically protected?, Proc. Natl. Acad. Sci. USA **113**, 8648 (2016).

[46] Q. Guo, B. Yang, L. Xia, W. Gao, H. Liu, J. Chen, Y. Xiang, and S. Zhang, Three Dimensional Photonic Dirac Points in Metamaterials, Phys. Rev. Lett. **119**, 213901 (2017).

[47] G. Li, B. Yan, Z. Wang, and K. Held, Topological Dirac semimetal phase in pd and pt oxides, Phys. Rev. B **95**, 035102 (2017).

[48] A. Slobozhanyuk, S. H. Mousavi, X. Ni, D. Smirnova, Y. S. Kivshar, and A. B. Khanikaev, Three-dimensional all-dielectric photonic topological insulator, Nat. Photon. **11**, 130 (2017).

[49] W. Yao, C. Li, L. Wang, S. Xue, Y. Dan, K. Iida, K. Kamazawa, K. Li, C. Fang, and Y. Li, Topological spin excitations in a three-dimensional antiferromagnet, Nat. Phys. **14**, 1011 (2018).

[50] M. Kargarian, Y.-M. Lu, and M. Randeria, Deformation and stability of surface states in Dirac semimetals, Phys. Rev. B **97**, 165129 (2018).

[51] S. Bao, J. Wang, W. Wang, Z. Cai, S. Li, Z. Ma, D. Wang, K. Ran, Z.-Y. Dong, D. Abernathy *et al.*, Discovery of coexisting dirac and triply degenerate magnons in a three-dimensional antiferromagnet, Nat. Commun. **9**, 2591 (2018).

[52] Q. Guo, O. You, B. Yang, J. B. Sellman, E. Blythe, H. Liu, Y. Xiang, J. Li, D. Fan, J. Chen, C. T. Chan, and S. Zhang,

Observation of Three-Dimensional Photonic Dirac Points and Spin-Polarized Surface Arcs, Phys. Rev. Lett. **122**, 203903 (2019).

[53] C. Le, X. Wu, S. Qin, Y. Li, R. Thomale, F.-C. Zhang, and J. Hu, Dirac semimetal in β-CuI without surface Fermi arcs, Proc. Natl. Acad. Sci. USA **115**, 8311 (2018).

[54] Y. Wu, N. H. Jo, L.-L. Wang, C. A. Schmidt, K. M. Neilson, B. Schrunk, P. Swatek, A. Eaton, S. L. Bud'ko, P. C. Canfield, and A. Kaminski, Fragility of Fermi arcs in Dirac semimetals, Phys. Rev. B **99**, 161113(R) (2019).

[55] P. Zhang, Z. Wang, X. Wu, K. Yaji, Y. Ishida, Y. Kohama, G. Dai, Y. Sun, C. Bareille, K. Kuroda *et al.*, Multiple topological states in iron-based superconductors, Nat. Phys. **15**, 41 (2019).

[56] Y. Yang, Z. Gao, H. Xue, L. Zhang, M. He, Z. Yang, R. Singh, Y. Chong, B. Zhang, and H. Chen, Realization of a three-dimensional photonic topological insulator, Nature (London) **565**, 622 (2019).

[57] S. M. Young, S. Zaheer, J. C. Y. Teo, C. L. Kane, E. J. Mele, and A. M. Rappe, Dirac Semimetal in Three Dimensions, Phys. Rev. Lett. **108**, 140405 (2012).

[58] Z. Wang, H. Weng, Q. Wu, X. Dai, and Z. Fang, Three-dimensional Dirac semimetal and quantum transport in Cd_3As_2, Phys. Rev. B **88**, 125427 (2013).

[59] K. Mullen, B. Uchoa, and D. T. Glatzhofer, Line of Dirac Nodes in Hyperhoneycomb Lattices, Phys. Rev. Lett. **115**, 026403 (2015).

[60] See Supplemental Material at http://link.aps.org/supplemental/10.1103/PhysRevResearch.4.033170. for a detailed topological surface-states discussion on the glide-protected topological invariant ν, the way to obtain Z_2 Dirac points in crystals, tight-binding model calculation for systems with Z_2 Dirac points and Z_2 Weyl dipole, and Weyl dipoles in other materials.

[61] L. Fu and C. L. Kane, Time reversal polarization and a Z_2 adiabatic spin pump, Phys. Rev. B **74**, 195312 (2006).

[62] H. Kim, K. Shiozaki, and S. Murakami, Glide-symmetric magnetic topological crystalline insulators with inversion symmetry, Phys. Rev. B **100**, 165202 (2019).

[63] H. Kim and S. Murakami, Glide-symmetric topological crystalline insulator phase in a nonprimitive lattice, Phys. Rev. B **102**, 195202 (2020).

[64] H. Kim, H. Cheng, L. Lu, and S. Murakami, Theoretical analysis of glide-z2 magnetic topological photonic crystals, Opt. Express **29**, 31164 (2021).

[65] L. Singh, V. Chopra, and S. P. Lochab, Synthesis and characterization of thermoluminescent $Li_2B_4O_7$ nanophosphor, J. Lumin. **131**, 1177 (2011).